

POD based reconstruction of subgrid stresses for wall bounded flows using neural networks

Christian Wollblad and Lars Davidson

Division of Fluid Dynamics, Department of Applied Mechanics,

Chalmers University of Technology,

Hörsalvägen 7b, SE41296 Gothenburg, Sweden

Fax: (+46)31-180976

Phone to corresponding author: (+46)31-7721408

E-mail to corresponding author: wollblad@chalmers.se

Abstract — A zonal hybrid method for computation of wall bounded flows was developed. Data from a direct numerical simulation of channel flow at Reynolds number 500 were filtered and the resulting subgrid stresses expanded in a series using proper orthogonal decomposition. The series was truncated. A feed forward neural network was found to be superior to linear stochastic estimation for estimating the coefficient of the series. The neural network and the orthonormal base from the expansion were shown by *a priori* tests to be suitable as a subgrid model for the innermost part of a boundary layer. The system was applied together with a Smagorinsky subgrid model to channel flow at Reynolds number 500 with good results. Generalization to higher Reynolds numbers is briefly discussed.

1. Introduction

The high computational cost of large eddy simulations (LES) for unsteady wall bounded flows makes alternative approaches attractive. A common technique is to use one computational method close to the wall and another in the outer region. These so called hybrid methods, or zonal methods, have been explored by for example Davidson and Peng [1], Hamba [2] and Tucker and Davidson [3] all of whom used some RANS model close to the wall up to some matching line and LES outside that line. The argument for these methods to work is that the LES and the RANS formulations of the Navier-Stokes equations are the same when the stress terms are expressed in terms of the turbulent viscosity, ν_t . Hence any model can be used for ν_t . LES is used away from walls since it provides good accuracy at a reasonable computational cost everywhere except for regions close to walls. Close to walls, RANS is the only feasible method for calculations at high Reynolds number and is thus applied there.

There are however conceptual problems with this approach. For plane channel flow, hybrid methods give a sudden increase in the mean streamwise velocity somewhere outside the matching line [1]. The reason is that RANS gives much higher values of ν_t and will therefore affect a much larger part of the turbulent spectrum while LES has levels of ν_t that damp only the smallest resolved scales. This will manifest itself as a jump in resolved turbulent scales at the matching line, as demonstrated in [4].

Some remedies have been suggested. Tucker and Davidson [3] used a one-equation $k - l$ model in both the RANS and LES regions and the regions differed in how the filter length scale was chosen. The results for plane channel flow improved if the transition from RANS to LES was made in a smooth manner instead of abruptly changing the filter length scale definition at the matching line. Several authors have used forcing at the matching line to reintroduce resolved LES scales from modeled RANS scales. See for example [5], [4], [6] and [7]. Hybrid

methods with forcing produce good mean velocity profiles for plane channel flows, but the forcing conditions are rather arbitrary. This is do some extent due to the problem pointed out by Temmerman et al. [8]: resolved turbulence is transported from the LES region into the RANS region, which responds by increasing the turbulent viscosity thus diminishing the effect of the forcing. This is however not always the case. In the work of Davidson and Billson [6], forcing resulted in a lower value of ν_t .

An alternative approach to the problem at the matching line is given by Hamba [2]. The value of ν_t on the RANS side of the matching line is much higher than on the LES side. To obtain the same level of ν_t on the LES side, the filter width has to be increased by approximately a factor 5, depending on the exact location of the matching line. However, the filter operator and the spatial derivatives in the Navier-Stokes equations do not commute in the mathematical sense but only to a second-order approximation in terms of the spatial derivative of the filter [9]. Hence, this rapid change in filter width will give rise to serious errors unless accounted for in some way. Hamba adopted a scheme with additional filtering of the data on the LES side of the matching line and obtained an improvement for computations of plane channel flow.

Since none of the suggested remedies works without a substantial amount of *ad hoc* adjustment, either the RANS method or the LES method has to be replaced. Since the main objective is to be able to make LES without completely resolving the boundary layer, it would be directly counterproductive to remove the LES part. It is therefore the RANS model that is discarded and replaced. In this work, data from direct numerical simulation (DNS) are filtered to give resolved velocities and subgrid stresses. The subgrid stresses close to walls are expanded using proper orthogonal decomposition (POD), which gives an orthonormal base for the subgrid stresses. Two different methods for recombining the base elements given some LES data are investigated, viz. linear stochastic estimation (LSE) and neural networks (NN).

For completeness, it should be mentioned that there exist related methods. For example, a RANS model can be used in the whole domain, but the level of ν_t is given an explicit dependence on the grid size. As the grid becomes coarse relative to the flow structures, for example in boundary layers, the method becomes equivalent to RANS, and when the grid becomes very fine compared to the flow structures, the method goes towards DNS, at least in theory. See for example [10] and [7]. Another alternative approach is to use a large eddy formulation in the whole domain, but instead of resolving the inner parts of the boundary layer, the first cell is made several hundred viscous units high. The wall is then accounted for by shear stress boundary conditions, often called approximate boundary conditions, which are computed in some way from the resolved velocity field. See for example [11] and [12].

2. Filtering of DNS data

Data are taken from a DNS of turbulent channel flow. The Reynolds number based on the friction velocity, u_τ , and channel half height, H , is 500 and the grid is Cartesian. The finite volume code is described in [1] and [13]. The resolution of the DNS is $\Delta x^+ = 49.1$, $\Delta z^+ = 12.3$ and $\min(\Delta y^+) = 0.3$. The wall normal stretching is 17%.

A box filter of streamwise and spanwise size $\Delta x^+ = 196$ and $\Delta z^+ = 49$ is used to obtain filtered data \bar{u}_i and \bar{p} and subgrid stresses $\tau_{ij}^{tot} = \overline{u_i u_j} - \bar{u}_i \bar{u}_j$. No filtering is done in the wall normal direction. The filter is thus 4×4 DNS cells and is 2×2 times larger than recommended for a well resolved LES [14]. A larger filter of 8×8 DNS cells was also tested but was discarded since the LES then became underresolved in terms of $\Delta x/H$.

In incompressible flow, the spherical part of the subgrid stress tensor $1/3 \tau_{kk}^{tot} \delta_{ij}$ is often included in the pressure. The current method is fully capable of modeling the total subgrid stress tensor

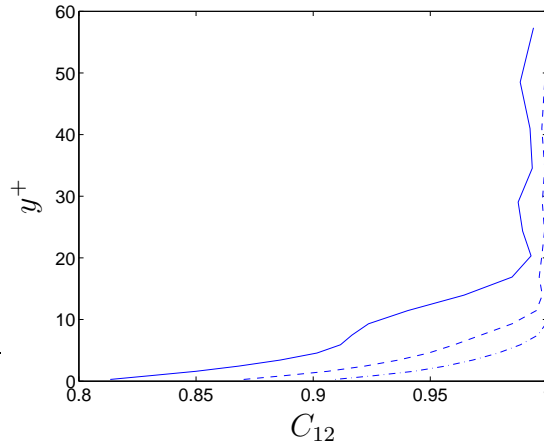


Figure 1: Correlation coefficient for τ_{12} and $\hat{\tau}_{12}$. —: $N = 20$, - - -: $N = 30$, - · - · -: $N = 40$

but, to avoid problems at the matching line, only the deviatoric part of the subgrid stress tensor, $\tau_{ij} = \tau_{ij}^{tot} - 1/3\tau_{kk}^{tot}\delta_{ij}$, will be modeled.

3. Proper orthogonal decomposition

POD is a method for expanding an arbitrary vector field, v_i , defined on a domain Ω in terms of a deterministic field $\phi_i = \sum_{n=1}^{\infty} \phi_i^n$. We want the orthonormal base $\{\phi_i^n\}_{n=1}^{\infty}$ to be optimal in the sense that the truncated projection

$$\hat{v}_i = \sum_{n=1}^N a^n \phi_i^n \quad (1)$$

is better than any other representation of v_i using the same number of basis functions. Optimality is measured by the projection $\langle |(v_i, \phi_i)| \rangle / \|\phi_i\|^2$ where (\cdot, \cdot) is the \mathcal{L}^2 inner product and $\langle \cdot \rangle$ is the assemble average. From calculus of variations, ϕ_i can be shown to be given as the solution to the eigenvalue problem

$$\int_{\Omega} \langle v_i(x)v_j(x') \rangle \phi_j(x') dx' = \lambda \phi_i(x) \quad (2)$$

and coefficients a^n are given by the projection

$$a^n = \int_{\Omega} v_i(x) \phi_i^n(x) dx \quad (3)$$

The basis functions, ϕ_i^n , are often referred to as POD modes and a^n as POD coefficients. More on POD can be found in [15] and [16].

The theory is here applied using τ_{ij} as the random field. The homogeneous directions x and z and the time are used for averaging and Ω is chosen to be $\{y^+ : y^+ \in [0, y_{max}^+]\}$. In this work y_{max}^+ is chosen to be equal to 62. For all $y^+ \leq y_{max}^+$ this gives the exact representation

$$\tau_{ij}(x, y, z, t) = \sum_{n=1}^{\infty} a^n(x, z, t) \phi_{ij}^n(y) \quad (4)$$

To make the representation effective, the series must be truncated. The accuracy of the truncated POD representation of τ_{ij} , denoted $\hat{\tau}_{ij}$, is measured using the correlation coefficient

$$C_{ij} = \frac{\langle (\hat{\tau}_{ij} - \langle \hat{\tau}_{ij} \rangle)(\tau_{ij} - \langle \tau_{ij} \rangle) \rangle}{\hat{\tau}_{ij,rms} \tau_{ij,rms}} \quad (5)$$

Figure 1 shows C_{12} for three different choices of N . As can be seen, truncation after 30 POD modes gives an accurate enough representation with very little improvement when more modes are added. The same trend can be seen for all elements of τ_{ij} . 30 modes is a relatively small number and can be compared to the number used in the work of P. Johansson [17]. He created a low-dimensional POD system to compute plane channel flow and used between 90 and 180 modes.

4. SGS reconstruction

To turn the (truncated) POD representation into a subgrid model, we ask the question 'what values do the POD coefficients assume for a given set of events $[h^1, \dots, h^M]$ '. The events are such that they can be calculated from filtered data, for example resolved velocity gradients. Two methods for calculating the most probable values of a^n given $[h^1, \dots, h^M]$ are investigated, linear stochastic estimation (LSE) and neural networks (NN).

LSE assumes a linear relationship between the fluctuations of the coefficients a^n and the values of $[h^1, \dots, h^M]$. The mapping matrix that minimizes the average square error, $\langle (\vartheta^n - a^n)^2 \rangle \forall n$, can be calculated exactly. ϑ^n is the approximation of a^n . The method is simple to implement and has a low computational cost. A more detailed description of LSE can be found in [18].

The theory of neural networks is far more complicated and the interested reader is referred to textbooks on the subject, such as [19]. The most important feature of NN is that they assume no functional form of the sought-after relation. The NN used in this work, a feed forward network with biases and two hidden layers, is in theory capable of reproducing any continuous function. The hidden layers use activation functions of the form $\tanh(v)$, where v is the weighted neuron input. The output layer uses pure linear activation functions. The mean is removed from both the input and output data of the network, but only the input data are normalized. The network is trained by the conjugate gradient algorithm with Polak-Ribière updates [20]. Half the available data set from the filtered DNS is used as the training set and the rest is split into a validation set and a cross-validation set.

Several different set of events were tested. Bagwell [21], who used LSE to construct approximate boundary conditions for LES, used an entire plane of the channel at constant y . Such a choice makes the method unsuitable for generalization to more complex geometries. Nicoud et al. [11], who used LSE for the same purpose, showed that more local events sufficed and that expanding the event field far in space did not give more accurate results. Therefore, the events for a column of cells with cell center points (x, y, z) , $y \in \Omega$ are kept as close to the column as possible. By trial and error, the following combination of events was found to give the best results without being too case specific:

$$\begin{aligned} u_i^+(x, y, z) & \quad \text{for } y^+ = y_{max}^+/2, y_{max}^+ \\ u_i^+(x \pm \Delta x, y, z) & \quad \text{for } y^+ = y_{max}^+/2, y_{max}^+ \\ u_i^+(x, y, z \pm \Delta z) & \quad \text{for } y^+ = y_{max}^+/2, y_{max}^+ \\ \partial P^+ / \partial z^+(x, y, z \pm \Delta z/2) & \quad \text{for } y^+ = y_{max}^+/2, y_{max}^+ \\ \partial P^+ / \partial y^+(x, y, z) & \quad \text{for } y^+ = 0, y_{max}^+/2, y_{max}^+ \end{aligned}$$

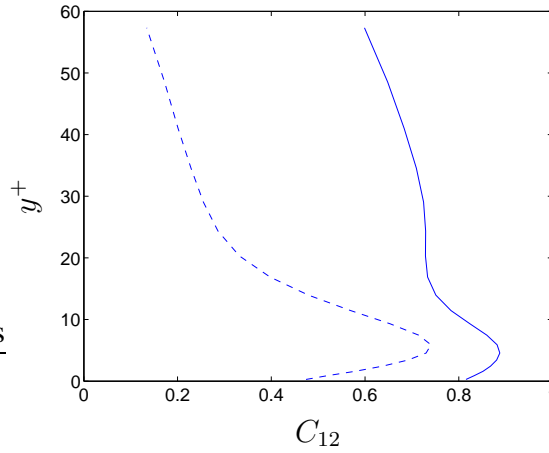


Figure 2: Correlation coefficient for τ_{12} and $\hat{\tau}_{12}^{NN}$ (—) and for τ_{12} and $\hat{\tau}_{12}^{LSE}$ (- - -)

$$\begin{aligned}
 \partial P^+ / \partial y^+(x \pm \Delta x, y, z) & \quad \text{for } y^+ = 0, y_{max}^+ / 2, y_{max}^+ \\
 \partial P^+ / \partial y^+(x, y, z \pm \Delta z) & \quad \text{for } y^+ = 0, y_{max}^+ / 2, y_{max}^+ \\
 \partial u^+ / \partial y^+(x, y = 0, z) & \quad \text{for } y^+ = 0 \\
 \partial u^+ / \partial y^+(x \pm \Delta x, y = 0, z) & \quad \text{for } y^+ = 0 \\
 \partial u^+ / \partial y^+(x, y = 0, z \pm \Delta z) & \quad \text{for } y^+ = 0 \\
 \partial w^+ / \partial y^+(x, y = 0, z) & \quad \text{for } y^+ = 0 \\
 \partial w^+ / \partial y^+(x \pm \Delta x, y = 0, z) & \quad \text{for } y^+ = 0 \\
 \partial w^+ / \partial y^+(x, y = 0, z \pm \Delta z) & \quad \text{for } y^+ = 0
 \end{aligned}$$

where Δx and Δz are the constant cell length and width. The pressure terms deserve some extra attention. Since $1/3\tau_{kk}^{tot}\delta_{ij}$ has been subtracted from the subgrid stress tensor, the term $1/3\rho\tau_{kk}^{tot}$ has to be added to the pressure when the LSE matrix and NN are created, i. e. $P = \bar{p} + 1/3\rho\tau_{kk}^{tot}$. Observant readers can also see that the events do not include any streamwise pressure gradients. This is to facilitate generalization. In calculations of pressure driven channel flow, the pressure gradient is often replaced by a force term, and the value of the streamwise pressure gradient will thus depend on the implementation. It is tempting to simply exclude the events based on pressure, but our investigation shows that both LSE and NN perform much better when events based on pressure are included than when they are not.

The number of events, M , is 59. 60 neurons in the first hidden layer and 40 neurons in the second hidden layer was the best configuration of those tested.

Both methods recover the mean values of the subgrid stresses almost perfectly. In figure 2 the untruncated subgrid stresses τ_{12} are compared with the reconstructed (and truncated) subgrid stresses calculated using coefficients estimated from LSE and from NN. The stresses estimated using LSE do not feature much higher correlation than subgrid stresses calculated with a Smagorinsky model. Stresses estimated from the neural network, however, feature much higher correlation with the real stresses and NN is hence a superior choice for reconstruction of the POD coefficients. This is confirmed by implementing LSE as described in section 6. Such a model diverges or gives horrible results. LSE will hence not be discussed further. Correlation coefficients C_{11} , C_{22} and C_{33} are all larger than C_{12} while the coefficients to the much less important τ_{13} and τ_{23} are somewhat smaller.

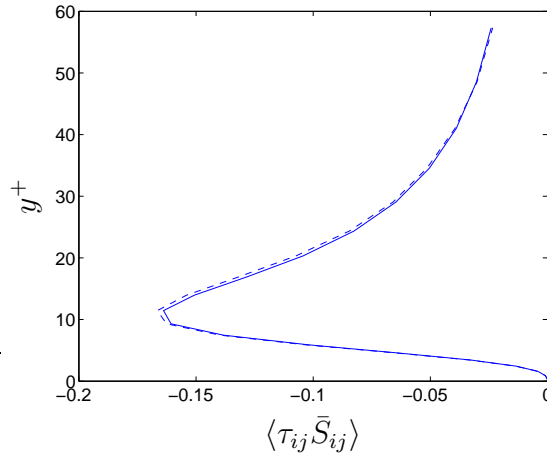


Figure 3: Transfer of turbulent kinetic energy to subgrid scales calculated using real stresses (—) and modelled stresses (---)

5. Subgrid model – a priori tests

In this work, a zonal approach is chosen where the POD-NN system is used as a subgrid model close to a wall while some LES subgrid model is used everywhere else. As a first step we consider simulation of the same flow from which the system was constructed, i. e. turbulent channel flow at Reynolds number 500 but with cells that are four times larger in the x and z directions than in the DNS calculation. The POD-NN system is used to calculate the subgrid stresses given a velocity field. This could be made in each iteration in any numerical scheme.

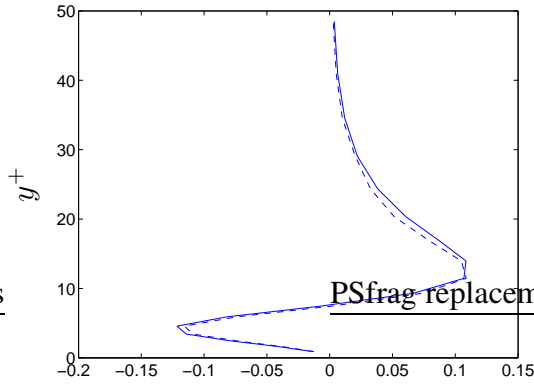
There are several necessary conditions that the system must fulfill in order to function as a subgrid model. One is to reproduce the averages of the subgrid stresses, and it has already been mentioned that it does. Another is to give a correct level of dissipation of turbulent kinetic energy to the subgrid scales, $-\tau_{ij}\bar{S}_{ij}$, where \bar{S}_{ij} is the resolved strain-rate tensor. Figure 3 shows $\langle \tau_{ij}\bar{S}_{ij} \rangle$ calculated using both the real τ_{ij} and using $\hat{\tau}_{ij}^{NN}$. As can be seen, the dissipation is well reproduced. This is a key requirement since the only reason that the Smagorinsky model works is that it reproduces the roughly correct level of dissipation to subgrid scales [22].

A subgrid model must also affect the resolved Reynolds stresses in a correct way. The spatially filtered velocity field, \bar{u}_i , can be decomposed into a time averaged component $\langle \bar{u}_i \rangle = U_i$ and a deviation from the time average, $\bar{u}_i - U_i = u'_i$. The transport equations for the resolved Reynolds stresses $\langle u'_i u'_j \rangle$ will contain the terms

$$-\langle u'_j \frac{\partial \tau'_{ik}}{\partial x_k} \rangle - \langle u'_i \frac{\partial \tau'_{jk}}{\partial x_k} \rangle \quad (6)$$

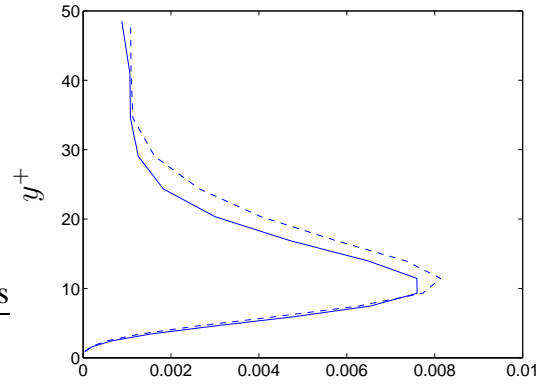
which represent all the effects of the subgrid stress tensor on the resolved Reynolds stresses [23]. Figures 4 and 5 show equation (6) for $\langle u'_1 u'_2 \rangle$ and $\langle u'_3 u'_3 \rangle$ calculated using the real stresses and the modeled stresses. Figure 4 is representative for the quality of equation (6) for $\langle u'_1 u'_1 \rangle$, $\langle u'_2 u'_2 \rangle$ and $\langle u'_1 u'_2 \rangle$, which are all strikingly good. Equation (6) is less well reproduced for $\langle u'_3 u'_3 \rangle$, but still good enough. This test shows that the POD-NN system reproduces the subgrid stress tensors well enough to be able to calculate its first-order spatial derivatives.

A priori tests like these shown so far can however only give indications of the system's ability to function as a subgrid model.



$$-\langle u'_2 \frac{\partial \tau'_{1k}}{\partial x_k} \rangle - \langle u'_1 \frac{\partial \tau'_{2k}}{\partial x_k} \rangle$$

Figure 4: Equation (6) for $\langle u'_1 u'_2 \rangle$ calculated using the real subgrid stresses (—) and modelled subgrid stresses (---)



$$-2\langle u'_3 \frac{\partial \tau'_{3k}}{\partial x_k} \rangle$$

Figure 5: Equation (6) for $\langle u'_3 u'_3 \rangle$ calculated using the real subgrid stresses (—) and modelled subgrid stresses (---)

6. Subgrid model – implementation and results

An incompressible, finite volume code with a non-staggered grid arrangement is used [1]. For space discretization, central differencing is used for all terms. The Crank-Nicholson scheme is used for time discretization of all equations. The numerical procedure is based on an implicit, fractional step technique with a multigrid pressure Poisson solver [24].

The Smagorinsky model is used in the center of the channel, i.e. further than 62 viscous units from the walls. The model constant, c_μ , is set to the standard value of 0.09 and the filter width is calculated by $\Delta = (\Delta x \Delta y \Delta z)^{1/3}$. Van Driest damping is applied. The POD-NN system is applied to the regions $y^+ \leq y_{max}^+$ and $2H - y \leq y_{max}^+$ where H is the channel half height. The divergence of the reconstructed subgrid stresses $\hat{\tau}_{ij}^{NN}$ are added as source terms to the discretized Navier-Stokes equations.

There are a few things that must be done to get a stable system. First, $\hat{\tau}_{ij}^{NN}$ needs to be under-relaxed to smooth its time history. If $\hat{\tau}_{ij}^{NN*}$ is the value from last iteration, the value used as a source term for the next iteration, $\hat{\tau}_{ij}^{NN**}$, is given by

$$\hat{\tau}_{ij}^{NN**} = c_r \hat{\tau}_{ij}^{NN}(u_i^*, P^*) + (1 - c_r) \hat{\tau}_{ij}^{NN*} \quad (7)$$

where $\hat{\tau}_{ij}^{NN}(u_i^*, P^*)$ is the value given by the POD-NN using the last known values of the velocity and pressure, u_i^* and P^* . Several values between 0.5 and 0.95 were tested for c_r and the results seem to be independent of the exact value. The only noticeable difference is that the numerical scheme becomes more unstable with higher values of c_r . The results shown later are calculated using $c_r = 0.8$. For consistency, the same amount of underrelaxation was applied to the Smagorinsky viscosity.

It is important that at least two iterations are made in each time step. If only one iteration is used, the lag between the velocity and the source terms created by the POD-NN system will create pressure fluctuations that grow an unlimited fashion. Neither extremely short time steps nor underrelaxation of $\hat{\tau}_{ij}^{NN}$ can make the scheme stable if only one iteration per time step is used.

If $\hat{\tau}_{ij}^{NN}$ is used to account for 100 % of the subgrid stresses in the regions close to the walls, the calculations eventually diverge. The measures described above lengthen the time before divergence and can even make the solution quasi-steady at solutions not far from the correct

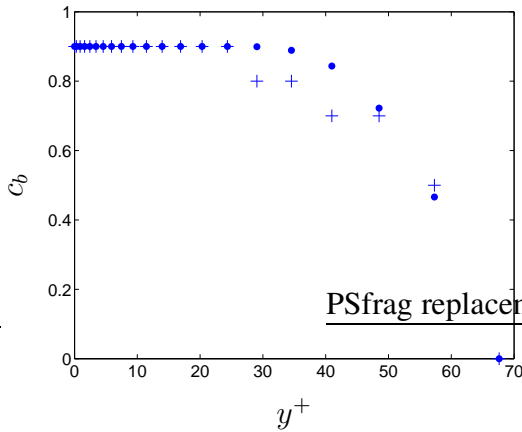


Figure 6: Two distributions of the blending coefficient, c_b . Solid dots mark distribution 1 and plus marks distribution 2.

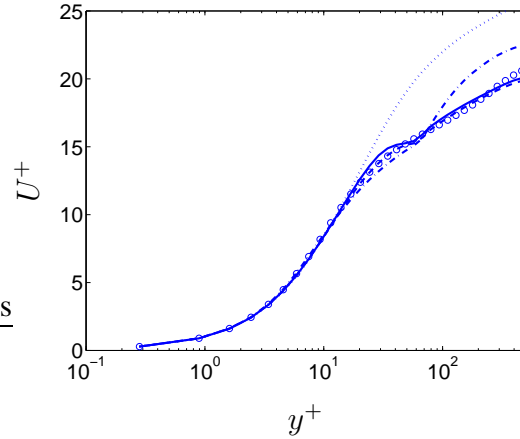


Figure 7: Velocity profiles for DNS ($\circ \circ \circ$), pure LES (\cdots), hybrid LES-RANS ($-\cdot-$) and POD-NN using distributions 1 ($—$) and 2 ($- - -$).

one. Stability can however be achieved by calculating the subgrid stresses by

$$\hat{\tau}_{ij} = c_b \hat{\tau}_{ij}^{NN} + (1 - c_b) \tau_{ij}^{Smag} \quad (8)$$

The blending coefficient, c_b , will be zero in the center region of the channel and non-zero in regions $y^+ \leq y_{max}^+$ and $2H - y \leq y_{max}^+$. It is possible to have c_b equal to a constant close to the walls but, since large values of c_b make the solution tend toward a pure Smagorinsky solution, the desire is to have c_b as close to one as possible. On the other hand, if c_b is constant close to one, there will be a sharp change in the approximation of τ_{ij} at the matching line, which creates a local velocity minimum there that can eventually destabilize the calculation. Therefore, c_b must be reduced in some way a few nodes before the matching line. Two different alternatives for c_b are shown in figure 6. Each marker represents a cell center and the distributions will be referred to as distributions 1 and 2 as described in the caption to the figure.

Figure 7 shows some velocity profiles, all with $u_\tau = 1.00$ and Reynolds number equal to 500. For reference, a solution using the Smagorinsky model in the whole domain, a DNS solution and a zonal RANS-LES solution with a one-equation $k - \ell$ model and the same matching line, are shown. The RANS-LES hybrid solution suffers from the deficiencies mentioned in the introduction, which results in too low resolved $\langle u'v' \rangle$ stresses. The pure Smagorinsky solution correctly predicts $\langle u'v' \rangle$ but its velocity profile overshoots since ν_t is too low for such a coarse grid. Two profiles calculated using the POD-NN system are shown, one for each distribution of c_b shown in figure 6. Both of these calculations give better results than the pure LES and the RANS-LES hybrid method. Distribution 2 gives a slightly smoother solution than distribution 1, but both profiles display a local retardation of the velocity at the matching line. Neither distribution 1 nor distribution 2 can be claimed to be optimal, but the results indicate that the method can be tuned to obtain an almost exact velocity profile.

Figures 8 and 9 compare resolved normal Reynolds stresses for the pure LES solution and the POD-NN solution using distribution 2. The stresses in figure 8 are typical for a poorly resolved LES with too high levels of streamwise stresses and too low levels of $\langle v'v' \rangle$ and $\langle w'w' \rangle$ stresses. Note that the DNS markers are the unfiltered Reynolds stresses and the LES stresses should hence fall below these curves, but not to the degree displayed in figure 8. The levels displayed

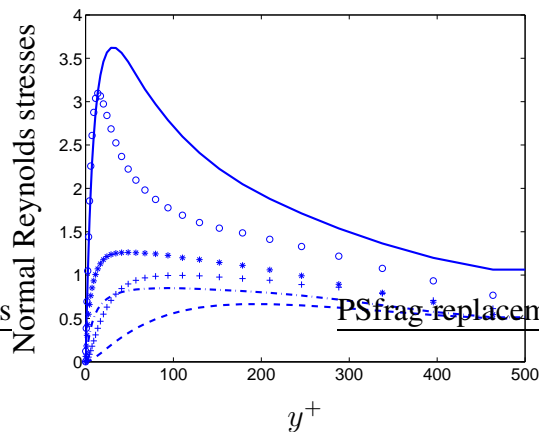


Figure 8: $\circ \circ \circ$, $* * *$ and $+ + +$ are $\langle u'u' \rangle$, $\langle w'w' \rangle$ and $\langle v'v' \rangle$ Reynolds stresses from DNS and —, $- \cdot -$ and $- - -$ are resolved $\langle u'u' \rangle$, $\langle w'w' \rangle$ and $\langle v'v' \rangle$ Reynolds stresses from the pure LES solution.

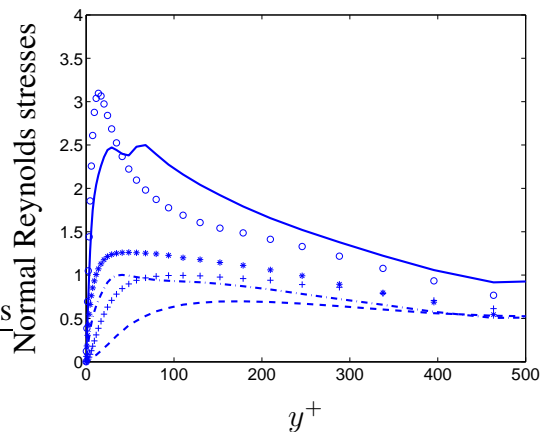


Figure 9: $\circ \circ \circ$, $* * *$ and $+ + +$ are $\langle u'u' \rangle$, $\langle w'w' \rangle$ and $\langle v'v' \rangle$ Reynolds stresses from DNS and —, $- \cdot -$ and $- - -$ are resolved $\langle u'u' \rangle$, $\langle w'w' \rangle$ and $\langle v'v' \rangle$ Reynolds stresses from the POD-NN calculation using distribution 2.

in figure 9 are much closer to what a filtered DNS solution looks like. The peak in the $\langle u'u' \rangle$ stress is located in the cell just outside the matching line. Despite the reduction of the blending coefficient, c_b , there will still be a huge gradient in the approximation of τ_{ij} which can be seen in equation (6) to give rise to an unphysically large production term in the $\langle u'u' \rangle$ equation and hence the extra peak in the $\langle u'u' \rangle$ stresses. This extra peak could have been removed by using a less aggressive reduction of c_b , but that would have been at the cost of a less good velocity profile. The only way to get around this problem is to move the matching line further from the wall. This however cannot be done using the current DNS at Reynolds number 500 since it is only the innermost 10 % of a boundary layer that is approximately universal [25]. Ten percent of the boundary layer thickness is in this case equal to $y^+ = 50$. This will be discussed further in section 7.

Figure 10 shows the resolved $\langle u'v' \rangle$ Reynolds stresses and $\langle \hat{\tau}_{12}^{NN} \rangle$. The total shear stress in the computations will be given by

$$\langle u'v' \rangle + c_b \langle \hat{\tau}_{12}^{NN} \rangle + (1 - c_b) \langle \tau_{12}^{Smag} \rangle + \langle \tau_{12}^{visc} \rangle \quad (9)$$

and for stress balance reasons will sum up to $1 - y$. For comparison, shear stresses from the DNS computation are also shown. Two features are especially prominent in figure 10. Firstly, due to the large filter $\hat{\tau}_{12}^{NN}$ is the dominant term in equation (9). Secondly, the fact that $\hat{\tau}_{12}^{NN}$ is not small near the matching line motivates the reduction of c_b in that region.

Figure 11 shows the resolved $\langle u'u' \rangle$ Reynolds stresses from DNS and POD-NN calculations using distribution 2 together with $\langle \hat{\tau}_{11}^{NN} \rangle$. Note that that $\hat{\tau}_{11}^{NN}$ approximates only the deviatoric part of the full subgrid stress element τ_{11}^{tot} . We know from the construction of the POD mode that $1/3\tau_{kk}^+ \approx 2$ where $\langle u'u' \rangle$ has its peak; with that information it is possible to deduce that the current method does not suffer as heavily as other hybrid methods from the so called *double counting* phenomenon, except in regions where the POD-NN system is not dominant. Double counting is effectively that resolved plus modeled turbulent kinetic energy is much higher than a DNS at the same Reynolds number and is more the standard than the exception in hybrid methods (see for example [6]).

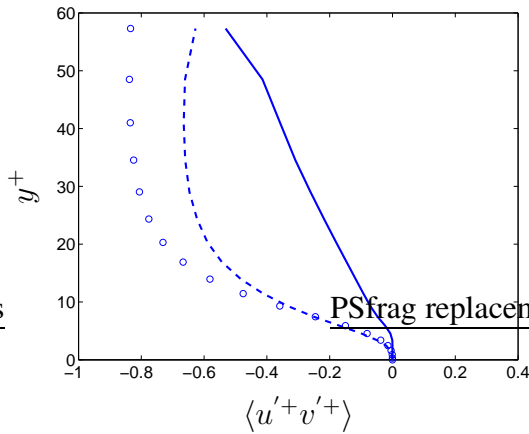


Figure 10: Shear stresses form DNS ($\circ \circ \circ$), resolved Reynolds stresses $\langle u'v' \rangle$ (—) and $\langle \tau_{12}^{NN} \rangle$ (---).

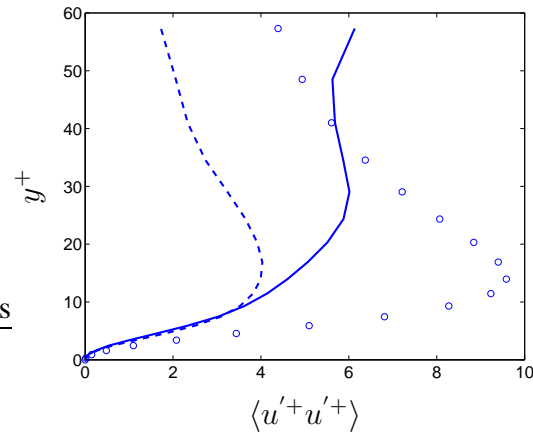


Figure 11: $\langle u'u' \rangle$ stresses form DNS ($\circ \circ \circ$), resolved Reynolds stresses $\langle u'u' \rangle$ (—) and $\langle \tau_{11}^{NN} \rangle$ (---).

The Reynolds stresses obtained using distribution 1 is very similar to those obtained using distribution 2 and are hence not shown.

7. Conclusions and future work

It has been shown that POD expansion of the deviatoric part of the subgrid stress tensor τ_{ij}^{tot} provides an orthonormal base that can be truncated at relatively low dimension. The POD coefficients are much better reproduced by a neural network than by linear stochastic estimation. *A priori* tests show that the POD-NN system should be functional as a subgrid model for cells close to a solid wall. Implementation in a finite volume code gave a system with some numerical difficulties, but very satisfactory results were obtained in the reproduction of the same channel flow from which the POD-NN system was created.

It is probable that the numerical stability, here obtained by underrelaxation and blending of the POD-NN system with the Smagorinsky model, could instead be obtained by regularization of the neural network. This however requires a deeper knowledge of NN theory than possessed by the authors.

For the model to be of any practical use, the POD modes must display some kind of Reynolds number independence, at least in a homeomorphic sense, as must the events used as input to the neural network. To investigate this matter a DNS of channel flow at Reynolds number 1000 was made. This DNS at higher Reynolds number will also enable us to increase y_{max}^+ to approximately 100, which will hopefully reduce the “jump” effects at the matching line. As mentioned in section 2 the limiting factor for the filter width is $\Delta x^+/H^+$. With a DNS at a doubled Reynolds number comes the possibility of testing larger values of Δx^+ .

Finally it is worth noting that a POD-NN could in theory be created and trained for any kind of flow close to walls. A suitable scaling other than the usual viscous scaling must then of course be used.

Acknowledgements

This project is sponsored by the Swedish Energy Agency.

References

1. Lars Davidson and Shia-Hui Peng. Hybrid LES-RANS: a one-equation SGS model combined with a $k - \omega$ model for predicting recirculating flows. *International Journal of Numerical Methods in Fluids*, 43:1003–1018, 2003.
2. Fujihiko Hamba. A hybrid RANS/LES simulation of turbulent channel flow. *Theoretical and Computational Fluid Dynamics*, 16:387 – 403, 2003.
3. P. G. Tucker and L. Davidson. Zonal $k - l$ based large eddy simulations. *Computers & Fluids*, 33:267 – 287, 2004.
4. J. Larsson, F. S. Lien, and E. Yee. Large eddy simulation of high Reynolds number channel flow on coarse grids. In *13th Annual Conference of the Computational Fluid Dynamics Society of Canada*, pages 61–68, St. Johns, Newfoundland, Canada, 2005.
5. Lars Davidson and Simon Dahlström. Hybrid LES-RANS: An approach to make LES applicable at high Reynolds number. *International Journal of Computational Fluid Dynamics*, 19:415–427, 2005.
6. L. Davidson and M. Billson. Hybrid LES-RANS using synthesized turbulent fluctuations for forcing in the interface region. *International Journal of Heat and Fluid Flow*, in print, 2006.
7. Ugo Piomelli, Elias Balaras, Hugo Pasinato, Kyle D. Squires, and Philippe R. Spalart. The inner-outer layer interface in large-eddy simulations with wall-layer models. *International Journal of Heat and Fluid Flow*, 24:538 – 550, 2003.
8. L. Temmerman, M. Hadžiabdić M. A. Leschziner, and K. Hanjalić. A hybrid two-layer URANS-LES approach for large eddy simulation at high Reynolds number. *International Journal of Heat and Fluid Flow*, 26:173 – 190, 2005.
9. Sandip Ghosal. Mathematical and physical constraints on large-eddy simulation of turbulence. *AIAA Journal*, 37:425 – 433, 1999.
10. Charles G. Spexiale. A combined large-eddy simulation and time-dependent RANS capability for high-speed compressible flows. *Journal of Scientific Computing*, 13:253 – 274, 1998.
11. F. Nicoud, J. S. Bagget, P. Moin, and W. Cabot. Large eddy simulation wall-modelling based on suboptimal control theory and linear stochastic estimation. *Physics of Fluids*, 13:2968 – 2984, 2001.
12. U. Piomelli, J. Ferziger, P. Moin, and J. Kim. New approximate boundary conditions for large eddy simulations of wall-bounded flows. *Physics of Fluids*, 1:1061, 1989.
13. Lars Davidson and Bijan Farhanieh. CALC-BFC A Finite-Volume Code Employing Collocated Variable Arrangement and Cartesian Velocity Components for Computation of Fluid Flow and Heat Transfer in Complex Three-Dimensional Geometries. Internal report 95/11, Chalmers University of Technology, Department of Thermo and Fluid Dynamics, Gothenburg, Sweden, 1995.
14. U. Piomelli and J.R. Chasnov. Large-eddy simulations: theory and applications. In D. Henningson, M. Hallbaeck, H. Alfredsson, and A. Johansson, editors, *Transition and Turbulence Modelling*, pages 269–336. Kulwer Academic Publisher, 1996.
15. Philip Holmes, John L. Lumley, and Gal Berkooz. *Turbulence, Coherent Structures, Dynamical Systems and Symmetry*. Cambridge Monographs on Mechanics, 1996.
16. William K. George. Some thoughts on similarity, the POD, and finite boundaries. In A. Gyr and A. Tsinober, editors, *Trends in Mathematics*, pages 117 – 128, 1998.
17. Peter Sassan Johansson. *Generation of inlet boundary conditions for numerical simulations of turbulent flows*. PhD thesis, Norwegian University of Science and Technology,

- 2004.
18. J. A. Taylor and M. N. Glauser. Towards practical flow sensing and control via POD and LSE based low-dimensional tools. *Journal of Fluids Engineering*, 126:337 – 345, 2004.
 19. Simon Haykin. *Neural Networks*. Prentice Hall International, Inc., international edition, 1999.
 20. <http://www.mathworks.com/access/helpdesk/help/toolbox/nnet/>. Matlab documentation web page, 2006.
 21. Ted Glyn Bagwell. *Stochastic Estimation of Near-Wall closure in Turbulence Models*. PhD thesis, Department of Nuclear Engineering, University of Illinois at Urbana-Champaign, 1994.
 22. Shewen Liu, Joseph Katz, and Charles Meneveau. Evolution and modelling of subgrid scales during rapid straining of turbulence. *Journal of Fluid Mechanics*, 387:281–320, 1999.
 23. Lars Davidson. Transport equations in incompressible URANS and LES. Internal report, 2006/01, Chalmers University of Technology, Department of Applied Mechanics, Division of Fluid Dynamics, Sweden, 2006.
 24. P. Emvin. *The Full Multigrid Method Applied to Turbulent Flow in Ventilated Enclosures Using Structured and Unstructured Grids*. PhD thesis, Dept. of Thermo and Fluid Dynamics, Chalmers University of Technology, Göteborg, 1997.
 25. Stephen B. Pope. *Turbulent flows*. Cambridge university press, Cambridge, United Kingdoms, 2000.